2013 IEEE/RSJ International Conference on
Intelligent Robots and Systems (IROS)
November 3-7, 2013. Tokyo, Japan

Force and Moment Generation of Fiber-reinforced Pneumatic Soft Actuators

Joshua Bishop-Moser, Girish Krishnan, and Sridhar Kota

Abstract*— *Soft actuators are found throughout nature from elephant trunks to round worms, demonstrating large specific forces without the need for sliding components. These actuators offer impact resilience, human-safe interaction, versatility of motion, and scalability in size. Biological structures often use a fiber-reinforcement around a fluid filled elastomeric enclosure, in which the elastomeric material will capture the distributed pressure and transfer it to the fibers, which will in turn direct the forces to the ends. We previously discovered an entire domain of fiber-reinforced elastomeric enclosures (FREEs), of which McKibben actuators are a small subset. The range of forces and moments possible with FREEs has not been previously investigated. 45 FREE actuators across the span of fiber angle configurations were fabricated and tested. The reaction force and moment of each actuator was determined across a gamut of pressures. Analytical models were generated using a variety of simplifying assumptions. These models were created to provide a closed form expression that models the force and moment data. The models were compared to the experimental values to determine their fit; this provides an understanding of which simplifying kinematic assumptions best represent the experimental results. Interpolated experimental results and the analytical models are all graphically represented for use as an intuitive design tool.

I. INTRODUCTION

Almost 90% of animal species lack a stiff backbone, yet impart tremendous forces on their prey or surroundings and are capable of dexterous and adaptable mobility patterns [1]. Engineers have tried to replicate these functionalities using artificial muscles made of soft constituents. One of the earliest configurations called the McKibben actuator or pneumatic artificial muscles [2] consists of a hollow elastomer tube reinforced with two families of symmetric helical fibers. Upon pressurization with fluids, these muscles contract or expand based on the fiber angle. A number of robots have been demonstrated using these muscles, described in review papers by Greef et al. [3], Trivedi et al. [4], and Webster et al. [5].

In our previous papers, we have generalized the construction of the McKibben actuator to include two families of asymmetrically would fibers capable of producing axial elongation and contraction, clockwise and counter-clockwise rotation, and their co-ordinated combination, i.e. screw motions [6] [7] [8] [9]. The kinematics of such a generalized actuator, named Fiber-Reinforced Elastomeric Enclosures (FREEs) have been predicted through reduced-order analytical modeling techniques that arise from the inextensibility of fibers and constant volume assumption of the fluids. However, the static and dynamic kinetic behavior is unknown for a all the configurations apart from the McKibben actuator subset.

Joshua Bishop-Moser is a Graduate Student in the Department of Mechanical Engineering, University of Michigan, Ann Arbor, MI 48109, USA joshbm@umich.edu

Girish Krishnan is a Post-doctoral Researcher in the Department of Mechanical Engineering, University of Michigan, Ann Arbor, MI 48109, USA gikrishn@umich.edu

Sridhar Kota is a Professor of Mechanical Engineering, University of Michigan, Ann Arbor, MI 48109, USA kota@umich.edu

This paper presents an experimental measurement and analytical verification of forces and moments that result upon pressurization of FREEs. Different FREEs with varying fiber angle configurations that correspond to equally spaced, non-redundant data points in the design space were fabricated using an in-house manufacturing process. Section II details the experimental methodology, while Section III illustrates the measurement results. The measured forces and moments are objectively compared against a unified analytical model based on the principle of virtual work. Section IV formulates this analytical model and compares it to the experimental results. Finally, the conclusion and contributions of the paper are summarized in Section V.

II. EXPERIMENTAL METHOD

A detailed understanding of the variables and parameters of the experiment are explored in Section II-A. The physical experimental setup is detailed in Section II-B. Section II-C explains the experimental procedure, including the points to be tested.

A. Variables and Parameters

The scope of this study encompasses cylindrical fiber-reinforced elastomeric enclosure (FREE) actuators that have two families of fibers, each with axial, circumferential, or helical fiber orientations. These fibers can be described using the fiber helix angles α and β with respect to the axial direction. Figure 1 shows the helical fiber angle notation for a FREE with two families of fibers. α and β can each range from $-90°$ to $90°$, providing a large design space to understand. Angles that are $90° < \alpha < 270°$ can be written as $(\alpha - 180°)$ and angles that are $270° < \alpha < 360°$ can be written as $(\alpha - 360°)$. This allows all fiber angles to be described using the $-90° < \alpha < 90°$ notation.

Half of the design space is redundantly labeled (e.g. $\alpha = 60°$, $\beta = 40°$ is the same configuration as $\alpha = 40°$, $\beta = 60°$ with the fiber labels switched). The design space of angle configurations is also symmetric about the $\alpha = -\beta$ line leading to axial forces that are equal, and moments that are equal in magnitude and opposite in direction. For example, the axial force will be the same for $\alpha = 30°$, $\beta = 70°$ as it will for $\alpha = -30°$, $\beta = -70°$, while the moment about the axial direction of the later will be equal in magnitude and opposite in direction to the former.

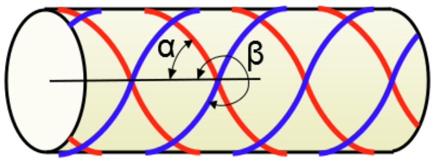

Fig. 1. Fiber-reinforced elastomeric enclosure (FREE) with 2 families of helical fibers at angles α and β. β can also be written as $(\beta - 360°)$. In this example α is approximately $45°$ and β is $-45°$.

A series of experiments were conducted to investigate the effect of helix angles α and β on the output variables of axial force (along its length) and moment generated about the axis. The radius parameter of the FREE actuators are fixed at 6 mm.

B. Experimental Setup

The test setup, shown in Figure 2, was used to measure the force and moment. The force was measured by a steel S beam resistive load cell (Loadstar RAS1-025S Resistive Load Cell, 25 Lbs capacity, $\pm 0.02\%$ FSO accuracy, universal mode digital calibration). The moment was measured with a reaction torque sensor (Loadstar RST1-006NM resistive torque sensor with 6 Nm max capacity, $\pm 0.2\%$ FSO accuracy, digital torsion calibration). Force and moment measurements were sent to the computer through two Loadstar DI-1000 Digital Load Cell Interface boxes. Off axis effect on each load cell (e.g. load on the torsion sensor and torsion on the load cell) were tested prior to experimentation and found to be negligible.

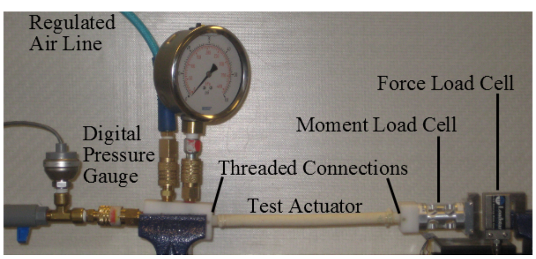

Fig. 2. Image of experimental setup with key components labeled.

Custom mounting brackets were fabricated to hold the load cells together in series. Additional custom connections were fabricated to provide a $\frac{1}{8}$ NPT tapped hole connecting the actuator being tested to the load cells on one end, and to the air inlet and pressure measurement on the other. The pressure was controlled manually from a regulated air compressor (Rigid 5-in-1 dual tank). The resulting pressure was measured using a digital pressure gauge (Cole Parmer 0 to 50 psig ± 0.25 PSI accuracy gauge transmitter, 0.5 to 5.5V output, P/N 68075-46). Measurements were sent to a computer using a Phidget 2/2/2 interface kit. An additional visual pressure gauge was attached to help with experimentation. The load cell setup and the pressure setup were fixed to a rigid surface using mounted clamps.

C. Experimental Procedure

The actuator for each test was installed by setting the distance between the threaded connections at the actuator's deflated length. The actuator was screwed into the threaded connection, with no rotation generated between the ends (i.e. the ends are in the same rotation as before they were screwed in). The ends were tightened enough to ensure no freedom to rotate, thus acting as fixed constraints. The pressure was manually increased, then held at numerous pressures up to the maximum safe pressure each actuator could withstand without failing or buckling (maximum pressure ranged from 100 to 275 kPa for the different actuators). The pressure was fixed until variables remained near constant over time, and the values at that point were recorded. Three sweeps were made from zero to maximum pressure, with measurements taken in each sweep.

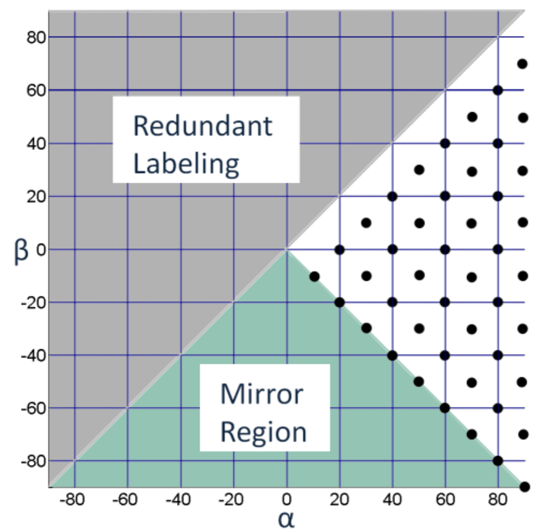

Fig. 3. α and β points tested shown as black dots (α and β in degrees). α and β combinations that are redundantly labeled are in the top left region, and α and β combinations that are mirror images of tested ones are in the bottom left.

As described in Section II-A, this paper investigates the effect of α and β on the force and moment generation. Only a quarter of this design space requires testing to understand all α and β combinations. A checkerboard pattern of 45 α, β combinations were selected for experimental testing, with the chosen values shown in Figure 3. Points very near the $\alpha = \beta$ line were not considered, as $\alpha = \beta$ points are degenerate cases that are underconstrained and will exhibit much different behavior than surrounding points. These points have an additional degree of freedom, which allows the actuators to inflate in an uncontrolled manner until failure.

III. Results

The direct results are processed to extract useful information from them, and this data processing is explored in Section III-A. The resulting experimental force measurements are shown in Section III-B, while the moment measurements are shown in Section III-C.

A. Data Processing

The force and moment measurements were highly linear with pressure for nearly all tests, most with an R^2 (coefficient of determination) over 0.990. The resulting slopes ($\frac{force}{pressure}$ and $\frac{moment}{pressure}$) were calculated for all tests, and these values were used for comparison across α and β values. The full force plot was obtained by mirroring the values collected in the quarter of the design space across the $\alpha = \beta$ and $\alpha = -\beta$ lines. The full moment plot was obtained by mirroring the values across the $\alpha = \beta$ line, then taking the negative of the values mirrored across the $\alpha = -\beta$ line.

A high resolution image was created from the data points by first interpolating the checkerboard pattern (seen in Figure 3) to a full grid of points spaced every $10°$ using a cubic interpolation. This grid of points was then interpolated three additional times using cubic interpolation to obtain a final high resolution grid (every $1.25°$) of force or moment per pressure values.

B. Experimental Force Results

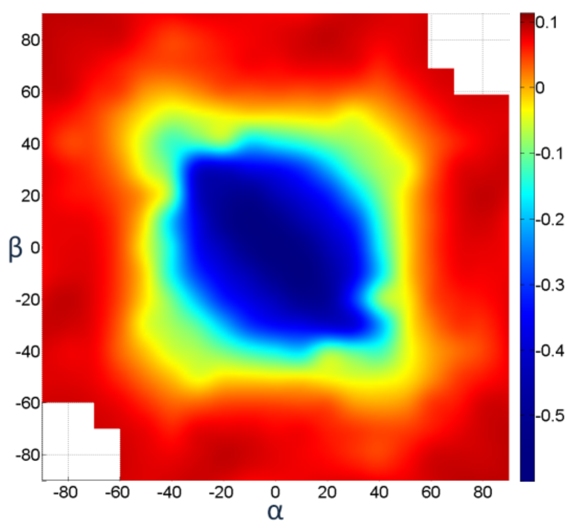

Fig. 4. Experimental force per pressure ($\frac{N}{kPa}$) across α and β (in degrees). Mirroring and cubic interpolation are used to obtain the entire design space from measured points seen in Figure 3. Radius set at 6mm.

The plot of the force normalized by pressure ($\frac{force}{pressure}$) across α and β helix angles (in degrees) is shown in Figure 4. Positive force indicates the actuator is exerting a force in the axial elongation direction, while negative is a contraction force. The normalized force is Newtons per kilopascal ($\frac{N}{kPa}$).

The force appears to take a square shape, with the forces trending towards contraction as α and β both head towards zero (fibers aligned along the axial direction). The square shape indicates that the fiber angle furthest from zero (closer to $90°$ or $-90°$) is driving the force term. An example of this effect is seen in Figure 4 where $\alpha = 10°$, $\beta = -80°$ has a similar force to $\alpha = 50°$, $\beta = -80°$, since the angle furthest from zero ($\beta = -80°$) is the same for both points. A more detailed analysis of this phenomenon is explored in Section IV-B.

The force crosses the zero line at approximately 54 degrees, which can be seen in orange in Figure 4. This aligns closely with existing knowledge about McKibben actuators that $\alpha = 54.4°$, $\beta = -54.4°$ is a configuration that produces no force when pressurized (The actuator will stiffen, but not exert force from its uninflated length). Beyond the $\alpha = 54.4°$, $\beta = -54.4°$ point, the entire McKibben actuator line of $\alpha = -\beta$ shows force values that align very closely with those expected from prior analysis and experimental work [10].

C. Experimental Moment Results

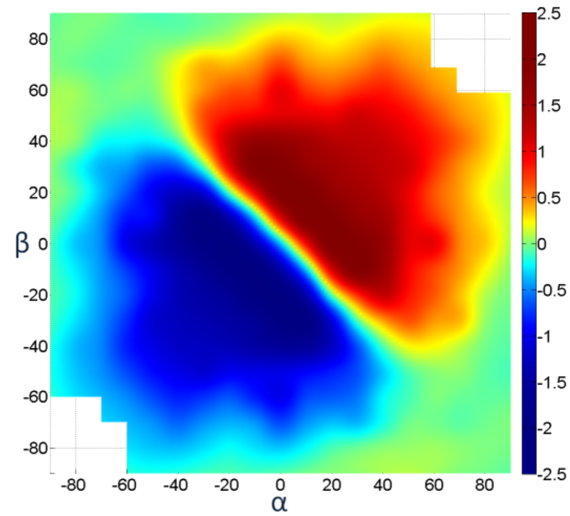

Fig. 5. Experimental moment per pressure ($\frac{N-mm}{kPa}$) across α and β (in degrees). Mirroring and cubic interpolation are used to obtain the entire design space from measured points seen in Figure 3. Radius set at 6mm.

The plot of the moment normalized by pressure ($\frac{moment}{pressure}$) across α and β helix angles (α and β in degrees) is shown in Figure 5. Positive moment indicates the actuator is exerting a moment in the counter-clockwise direction when viewed from the actuator facing outward, while negative is a clockwise moment, again from the middle of the actuator looking towards the ends. The normalized moment is Newton-millimeters per kilopascal ($\frac{N-mm}{kPa}$).

The moment plot takes a complicated shape that will be explored in more detail in Section IV-A. One region in which the moment reaches zero is down the $\alpha = -\beta$ line, seen in green. This aligns closely with existing knowledge that McKibben actuators ($\alpha = -\beta$) produce no moment when pressurized (The actuator will stiffen, but not exert moment from its deflated length and rotation).

IV. Analytical Modeling

We have performed previous work on modeling fiber reinforced elastomeric enclosure (FREE) actuators to understand their kinematics [9], as well as their force and moment behavior [6]. The axial and radial deformation of a cylinder are expressed as stretch ratios λ_1 and λ_2 respectively. θ is the number of rotations of the fiber in radians, and θ^* the rotations after deformation, with the difference describing the cylinder rotation as angle δ. The volume enclosed within the cylinder before deformation is V, and V^* after deformation.

Equation 1 describes the inextensibility of a fiber, which is found by setting the length of the fiber before and after actuation to be equal. Equation 2 describes the volume after actuation; the unactuated volume is $V = \pi r^2 l$. Equation 3 shows the equation for the number of rotations that a fiber will make while spiraling the length of an unactuated FREE. Equation 4 shows the rate of volume change with respect to λ_1, and Eq. 5 shows the pitch (height change per rotation) of the actuator during inflation. These equations provide an understanding of the volume change per motion, or hydraulic displacement amplification, which can be combined with the principle of virtual work to obtain force and moment.

$$\lambda_1^2(\cos\alpha)^2 + \lambda_2^2(\sin\alpha)^2(\frac{\theta^*}{\theta})^2 = 1 \tag{1}$$

$$V^* = \lambda_2^2\lambda_1\pi r^2 l \tag{2}$$

$$\theta = \frac{tan(\alpha)l}{r} \tag{3}$$

$$\lim_{\lambda_1\to 1}\frac{dV}{d\lambda_1} = (1+2\cot(\alpha)\cot(\beta))\pi r^2 l \tag{4}$$

$$p = \frac{r\sin(\alpha)\sin(\beta)\sin(\alpha-\beta)}{(\sin(\alpha)^2 - \sin(\beta)^2)} \tag{5}$$

A. Moment Model

The underlying assumption for the moment model is that virtual work can be applied to the volume expansion per unit motion of a FREE actuator to determine the magnitude of the moment exerted. The kinematics of the *unconstrained* FREE will determine the direction of the force and moment, including the relative magnitude of the force and moment terms. This relationship is governed by the pitch, seen in equation 5. Equation 6 shows how the moment term can be derived starting from the virtual work equation, leading to the full expression of the moment in equation 7. The figure for this model is shown in Figure 6.

$$PdV = Fdl + Md\delta \tag{6}$$

$$PdV = \frac{M}{q}ld\lambda_1 + M\frac{ld\delta}{p} = Mld\lambda_1(\frac{p}{r^2}+\frac{1}{p})$$

$$where: q = \frac{r^2}{p}$$

$$M = \frac{P}{l}\frac{dV}{d\lambda_1}\frac{1}{p+\frac{r^2}{p}}$$

$$M = \frac{P}{l}(1+2\cot(\alpha)\cot(\beta))\pi r^2 l\frac{pr^2}{r^2+p^2}$$

$$M = P\frac{\pi r^3(1+2\,Ct_\alpha\,Ct_\beta)\,S_\alpha\,S_\beta\,S_{\alpha-\beta}\,(S_\alpha^2 - S_\beta^2)}{S_\alpha^2\,S_\beta^2\,S_{\alpha-\beta}^2 + (S_\alpha^2 - S_\beta^2)^2} \tag{7}$$

$$where: S_x = \sin(x),\, Ct_x = \cot(x)$$

The moment model appears to accurately predict the experimental values. To verify the quality of the prediction, the residuals were computed for all points, and is seen in Figure 7. The residual is largest in the region near the $\alpha = \beta$ line, which as discussed in Section II-C, were not tested, as these actuators have a tendency to expand uncontrollably. The remaining regions have a low residual, with exceptions from a few data points, implying this analytical model is a very good representation of the experimental data. This further shows that the model assumption of using the unconstrained kinematics and the volume change per motion with virtual work accurately reflects the behavior of a constrained, actuated FREE in moment generation.

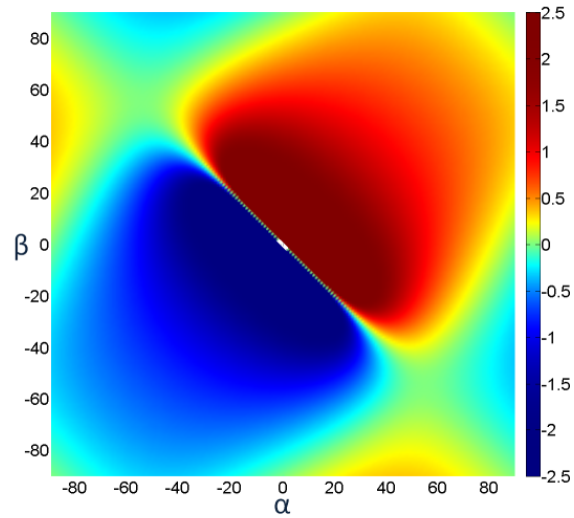

Fig. 6. Analytical model of the moment per pressure ($\frac{N-mm}{kPa}$) across α and β (in degrees). Radius set at 6mm.

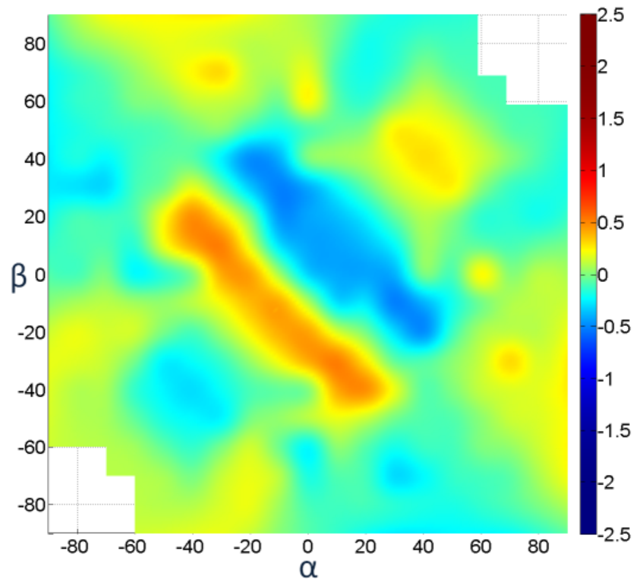

Fig. 7. Residual of the experimental and analytical model of the moment per pressure ($\frac{N-mm}{kPa}$) across α and β (in degrees). Radius set at 6mm.

B. Force Model

Similar to the moment model, the force model assumes that the volume expansion per unit motion, through virtual work, determines the magnitude of the force. For the force model, two different additional assumptions will be considered. In Model #1, the assumption that the kinematics of the *unconstrained* FREE will determine the direction of the force and moment will be again used. Model #2 uses a different assumption, that the kinematics are determined using a *constrained rotation* that is fixed at zero (no rotation). The resulting change in volume will be driven by pure linear motion, in this case the negative of compressive motion. Note that additional models can be created by modifying any of these assumptions. The relative magnitude of the force to the moment terms in Model #1 is governed by the pitch, while for Model #2, the compression will lead to one family of fibers buckling, while the other one drives the motion.

This simple change in assumptions, from unconstrained kinematics to constrained rotation will substantially alter the resulting force model. Model #1 is derived in a similar manner to the moment model (equations 6 and 7), but for force instead, which is seen in equation 8. The figure for Model #1 is shown in Figure 8. The derivation for Model #2 is shown in equation 9, where $\frac{dV}{d\lambda_1}$ only acts in the force direction, since the rotation, and consequently volume change, is fixed at zero for rotation.

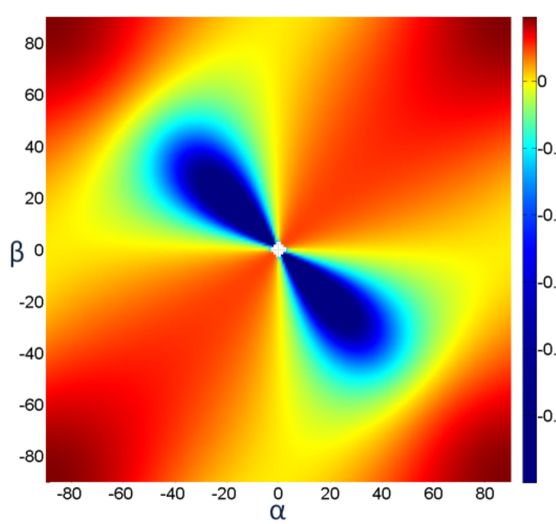

Fig. 8. Analytical Model #1 of the force per pressure ($\frac{N}{kPa}$) across α and β (in degrees). Radius set at 6mm. Model #1 assumes unconstrained kinematics drives the volume change magnitude and resulting force magnitude and direction.

$$
\begin{aligned}
PdV &= Fdl + Md\delta = Fld\lambda_1 + M\frac{ld\delta}{p} \\
PdV &= Fld\lambda_1 + Fq\frac{ld\delta}{p} = Fld\lambda_1(1 + \frac{r^2}{p^2}) \\
&where: q = \frac{r^2}{p}
\end{aligned}
$$

$$
\begin{aligned}
F &= \frac{P}{l}\frac{dV}{d\lambda_1}\frac{1}{1+\frac{r^2}{p^2}} \\
F &= \frac{P}{l}(1 + 2\cot(\alpha)\cot(\beta))\pi r^2 l\frac{p^2}{r^2+p^2} \\
F &= P\frac{\pi r^2(1 + 2\,Ct_\alpha\,Ct_\beta)\,S_\alpha^2\,S_\beta^2\,S_{\alpha-\beta}^2}{S_\alpha^2\,S_\beta^2\,S_{\alpha-\beta}^2 + (S_\alpha^2 - S_\beta^2)^2} \\
&where: S_x = \sin(x),\, Ct_x = \cot(x)
\end{aligned}
\tag{8}
$$

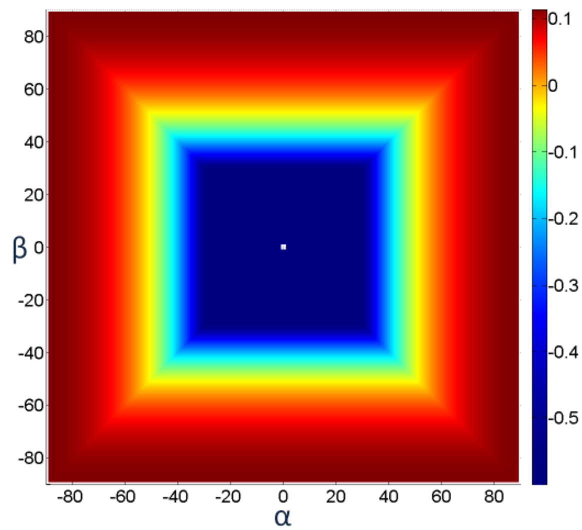

Fig. 9. Analytical Model #2 of the force per pressure ($\frac{N}{kPa}$) across α and β (in degrees). Radius set at 6mm. Model #2 assumes kinematics of fibers with a fixed rotation drives the volume change magnitude and resulting force magnitude and direction.

$$
\begin{aligned}
\lambda_1^2(\cos\gamma)^2 + \lambda_2^2(\sin\gamma)^2(\frac{\theta^*}{\theta})^2 &= 1 \\
\delta = 0 \implies \frac{\theta^*}{\theta} &= 1 \\
V^* = (\csc(\gamma)^2\lambda_1 - \cot(\gamma)^2\lambda_1^3)\pi r^2 l \\
\lim_{\lambda_1\to 1}\frac{dV}{d\lambda_1} &= \pi r^2 l(1 - 2\cot\gamma^2) \\
PdV = Fdl = Fld\lambda_1 \implies F &= P\frac{dV}{ld\lambda_1} \\
F &= P\pi r^2(1 - 2\cot(\gamma)^2)
\end{aligned}
\tag{9}
$$

where: γ is α or β that is further from zero

Force Model #2 appears to closely predict the experimental values, while Model #1 substantially deviates. This shows that the assumption underlying Model #2, of using the fixed rotation and the negative volume change of compression, accurately reflects the behavior of a constrained, actuated FREE in force generation. This result is non-intuitive, as the assumptions that underlie the force model are different from those that represent the experimental moment values. To verify the quality of the prediction for Model #2, the residual was computed for all points, and is seen in Figure 10. The residual is largest in the region near the $\alpha = \beta$ line, which as discussed in Section II-C, were not tested for. The

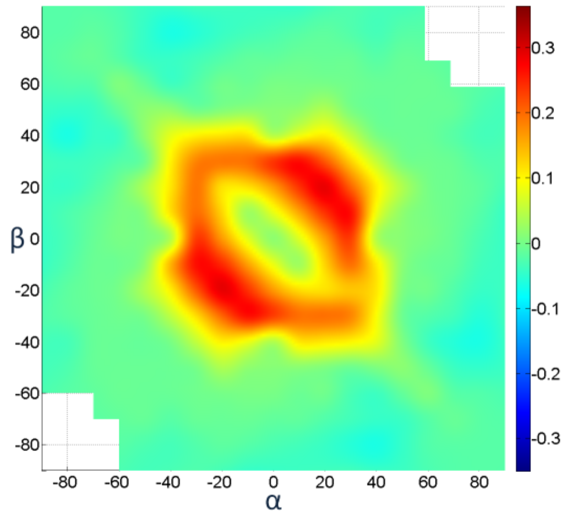

Fig. 10. Residual of the experimental and analytical Model #2 of the force per pressure ($\frac{N}{kPa}$) across α and β (in degrees). Radius set at 6mm.

remaining regions have a low residual, with exceptions from a few data points, implying this analytical model is a very good representation of the experimental data.

V. Conclusions

This paper experimentally determines the force and moment generation for FREEs with two families of fibers across the entire design space using a blocking-load based test. Kinematics was used in conjunction with virtual work to determine analytical models of the force and moment generation for comparison with the experimental results. The kinematics of an unconstrained actuator best predict the moment generation, while the kinematics of a rotation constrained, compressive load best predict the force generation. The results also compared favorably to existing research on McKibben actuators. The primary contributions of this paper are

1) Experimental determination of the force and moment for FREEs with two families of fibers.
2) Analytical model of the force and moment of FREEs, including an exploration of the underlying assumptions of the kinematic model.
3) Graphical representation of the design space, allowing for fast and intuitive understanding of how to synthesize FREEs for desired force and moment.

The experimental and analytical model plots provide a way to quickly understand the range of possible designs to synthesize a FREE for a given force and/or moment. They also allow a designer to understand the sensitivity of the design to changes in fiber angle. By addressing the full range of FREEs, beyond just McKibben actuators, a wide range of actuation types are possible, including pure moment and every type of wrench (combination of moment and force). The application of this knowledge expands beyond just engineered structures, as the many biological examples that inspire this research can be better understood using the provided relationship between fiber angle and volume with force and moment.

A. Future Work

The experimental method captured the force and moment generated with a blocking load. Additional tests that relax various constraints, such as only blocking elongation or prescribing a linear sweep of rotation values will enable a better understanding of the forces and moments for a broader range of external conditions. This understanding will also work towards the goal of being able to control the actuators dynamically. Another future direction is to use a regression model that generates a lower order model directly from the experimental data. This will be useful for providing an analytical model that is obtained directly from experiment, rather than kinematic approximations. The analytical model used was made under the assumption that material does not affect the outcome and all kinematics are non-linear. By using a blocking load test, these assumptions do not cause much error, but for even higher accuracy including a material model and non-linearities are important next steps. Additionally, experiments in which the actuator is allowed to deform will necessitate a material model.

VI. Acknowledgements

The authors would like to acknowledge the assistance of Darlene Yao and Corey Bertch. This work was supported by the National Science Foundation under NSF Award 1030887 and the Graduate Research Fellowship.

References

[1] S. Vogel, Comparative Biomechanics. Princeton, New Jersey: Princeton, 2003.

[2] Gaylord, R., 1958. ‘Pressure source,’ July 22. US Patent 2,844,126.

[3] A. DeGreef, P. Lambert, and A. Delchambre, ‘Towards Flexible Medical Instruments: Review of Flexible Fluidic Actuators,’ *Precision Engineering*, Vol. 33, No. 4, pp. 311-321, Oct. 2009.

[4] D. Trivedi, C. Rahn, W. Kierb, and I. Walker, ‘Soft Robotics: Biological Inspiration, State of the Art, and Future Research,’ *Applied Bionics and Biomechanics*, Vol. 5, No. 3, pp. 99 - 117, Sept. 2008.

[5] R. J. Webster III, and B. Jones, ‘Design and Kinematic Modeling of Constant Curvature Continuum Robots: A Review,’ *Int. J. of Robotics Research*, Vol. 29, No. 13, pp. 1161 - 83, Nov. 2010.

[6] J. Bishop-Moser, G. Krishnan, and S. Kota, ‘Force and Hydraulic Displacement Amplification of Fiber Reinforced Soft Actuators,’ *ASME Conference Proceedings, 2013.*

[7] J. Bishop-Moser, G. Krishnan, C. Kim, and S. Kota, ‘Design of Soft Robotic Actuators Using Fluid-filled Fiber-reinforced Elastomeric Enclosures in Parallel Combinations,’ *Intelligent Robots and Systems (IROS), 2012 IEEE/RSJ International Conference on*, vol., no., pp.4264,4269, 7-12 Oct. 2012.

[8] J. Bishop-Moser, G. Krishnan, C. Kim, and S. Kota, ‘Kinematic Synthesis of Fiber Reinforced Soft Actuators in Parallel Combination,’ *Proceedings of the 36th Mechanisms and Robotics Conference at ASME IDETC 2012*, Chicago, IL, August 2012.

[9] G. Krishnan, J. Bishop-Moser, C. Kim, and S. Kota, ‘Evaluating Mobility Behavior of Fluid Filled Fiber- Reinforced Elastomeric Enclosures,’ *Proceedings of the 36th Mechanisms and Robotics Conference at ASME IDETC 2012*, Chicago, IL, August 2012.

[10] B.Tondu and P.Lopez, ‘Modeling and control of McKibben artificial muscle robot actuators,’ Control Systems, IEEE , vol.20, no.2, pp.15,38, Apr 2000.